# Lattice location and thermal stability of implanted nickel in silicon studied by on-line emission channeling

D. J. Silva,[1] U. Wahl,[2] J. G. Correia,[2] L. M. C. Pereira,[3] L. M. Amorim,[3] M. R. da Silva,[4] E. Bosne,[2,5] and J. P. Araújo[1,a)]

[1)] *IFIMUP and IN-Institute of Nanoscience and Nanotechnology, Departamento de Física e Astronomia da Faculdade de Ciências da Universidade do Porto, 4169-007 Porto, Portugal*

[2)] *Centro de Ciências e Tecnologias Nucleares, Instituto Superior Técnico, Universidade de Lisboa, 2686-953 Sacavém, Portugal*

[3)] *Instituut voor Kern- en Stralingsfysica, KU Leuven, 3001 Leuven, Belgium*

[4)] *Centro de Física Nuclear da Universidade de Lisboa, 1649-003 Lisboa, Portugal*

[5)] *Departamento de Física da Universidade do Aveiro, 3810-193 Aveiro, Portugal*

(Dated: 16 December 2013)

We have studied the lattice location of implanted nickel in silicon, for different doping types ($n$, $n^+$ and $p^+$). By means of on-line emission channeling, $^{65}$Ni was identified on three different sites of the diamond lattice: ideal substitutional sites, displaced bond-center towards substitutional sites (near-BC) and displaced tetrahedral interstitial towards anti-bonding sites (near-T). We suggest that the large majority of the observed lattice sites are not related to the isolated form of Ni but rather to its trapping into vacancy-related defects produced during the implantation. While near-BC sites are prominent after annealing up to 300-500°C, near-T sites are preferred after 500-600°C anneals. Long-range diffusion starts at 600-700°C. We show evidence of Ni diffusion towards the surface and its further trapping on near-T sites at the $R_p/2$ region, providing a clear picture of the microscopic mechanism of Ni gettering by vacancy-type defects. The high thermal stability of near-BC sites in $n^+$-type Si, and its importance for the understanding of P-diffusion gettering are also discussed.

CERN-OPEN-2014-018
17/12/2013

## I. INTRODUCTION

The search for more reliable silicon-based technologies has been hampered by the presence of transition metals (TMs) as contaminants. Because TMs act as recombination centers, due to the introduction of deep levels in the silicon bandgap, the reduction of minority carrier lifetime hinders, e.g., the efficiency of silicon solar cells, even when TMs are present at low concentrations.[1–4] Together with copper, nickel is an ultrafast diffuser in Si, with an often quoted activation energy for diffusion of $E_D = 0.47$ eV,[5] which has recently been proposed to be as low as 0.15 eV.[6] Although being one of the less studied, Ni is one of the most harmful TMs. Efforts have been made to both passivate its malicious electrical effect with, e.g., hydrogenation,[7] or by moving the Ni impurity away from the active area of the device with the so called gettering procedures, such as by trapping Ni into defects[8,9] or use P-diffusion to getter Ni into $n^+$ rich regions.[10,11]

Calculations have concluded that interstitial tetrahedral Ni does not have energy levels in the Si bandgap.[5,6] The reason for its harmful effect comes from the fact that the solubility of the harmless and fast diffusing interstitial nickel is so small[12] that it is normally trapped into defects, forming, in particular, electrically active silicides when agglomeration of Ni takes place.[1,11,13] The introduction of deep levels by nickel contamination will thus depend on its ability to form complexes with other defects. Although the information is scarce, a way to distinguish different complexes is by observing the different lattice sites of Ni. For instance, single vacancies will in principle trap Ni atoms on substitutional sites[5,6] while divacancies might trap Ni on other sites, e.g. bond-center sites. Moreover, the microscopic picture of Ni gettering by defects and the mechanism of P-diffusion gettering are still not yet well understood. The knowledge of the lattice sites of Ni might thus provide crucial information for the clarification of such complex mechanisms.

Beta emission channeling (EC) is a unique technique to investigate the preferred lattice sites of low concentrations of impurities following implanting single crystals with radioactive probe atoms which decay by emitting $\beta^-$ particles. On their way out of the crystal, $\beta^-$ particles experience channeling effects along low-index crystallographic directions, depending on the lattice site occupied by the probe atom. EC has been used to study the lattice sites of long-lived TM isotopes in Si, such as $^{67}$Cu ($t_{1/2}$=2 d),[14–17] $^{59}$Fe (45 d)[17–19] and $^{111}$Ag (7.45 d),[20] by means of off-line experiments. Studies of other TMs, in particular Ni, Co and Mn, were not feasible since the only suitable isotopes were too short-lived in order to be used off-line. However, this situation has recently changed with the installation of an on-line EC setup at the isotope mass separator facility ISOLDE at CERN.[21] This online setup has allowed to study the lattice location of: $^{56}$Mn ($t_{1/2} = 2.56$ h) in Ge,[22] GaAs,[23,24] GaN,[25] and ZnO;[26] $^{61}$Co (1.6 h) in ZnO;[26] and $^{65}$Ni (2.5 h) in ZnO.[27]

Since Ni is a very fast diffuser, only the interaction

[a)] jearaujo@fc.up.pt

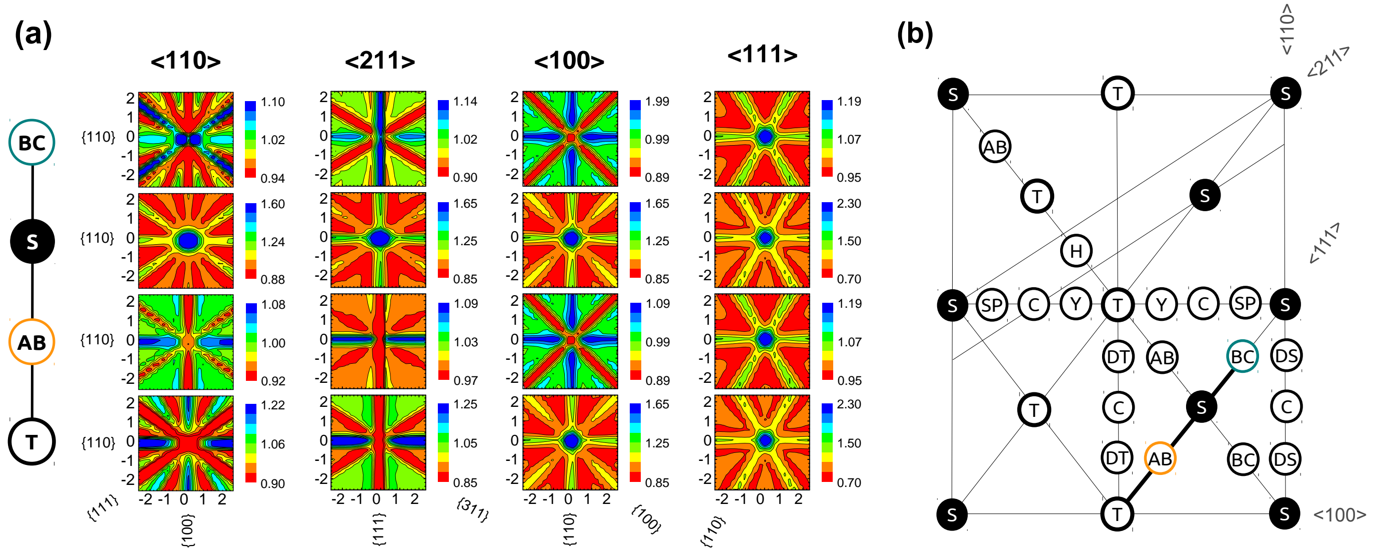


FIG. 1. (Color online) (**a**) Theoretical beta emission yield patterns for the sequence of sites along the <111> direction, BC → S → AB → T, around <110>, <211>, <100> and <111>. The patterns of S sites are characterized by channeling peaks from all the four orientations shown. On the contrary, the channeling peaks from <211> and <100> are absent in the patterns of BC sites. While exhibiting channeling effects along {111} planes, the beta emission yields of BC sites show blocking effects along {100} and {311}. Moreover, BC sites are characterized by a double peak along <110>. Both the patterns of T and AB sites present blocking effects of the {111} planes, but while the patterns of T sites show peaks from <100> and {100}, patterns of AB sites show blocking effects along these axis and planes. (**b**) Positions of the major sites in the silicon lattice, shown in the {110} plane.

with defects, such as other impurities, other Ni atoms, self-interstitials or vacancy-type defects, can immobilize Ni atoms even at room temperature. Anyhow, the properties of Ni as a fast diffuser might influence which traps are preferred. For instance, isolated interstitial nickel prevails in the neutral charge state, which makes its interaction with immobile charged dopants unlikely. In fact, the formation of pairs driven by Coulomb interactions, e.g. NiB, have not been experimentally reported. On the contrary, while pairing with Si interstitials is also not expected,[6] neutral Ni can be effectively trapped by vacancies. Indeed, clusters of vacancies are one of the most effective gettering centers.[9,28] In that respect, defects in irradiated silicon have been reported to getter Ni in two different regions: around the peak concentration of the implanted Ni, known as the $R_p$ region, and midway between the peak concentration and the surface, known as the $R_p/2$ region.[8,29,30] It was suggested by positron annihilation spectroscopy that the latter region might correspond to the vacancy peak concentration produced by the implanted Si.[31,32].

Changing the doping type may also influence the preferred sites of Ni since the stability of its various configurations are directly coupled to the electron-hole charge equilibrium. Although isolated tetrahedral interstitial nickel has no acceptor neither donor levels in the silicon bandgap, other configurations have the possibility to be electrically active. For instance, substitutional nickel has two acceptor levels close to the conduction band, $E_\mathrm{C}$ - 0.09 eV and $E_\mathrm{C}$ - 0.43 eV, and one donor level close to the valence band, $E_\mathrm{V}$ + 0.17 eV.[5,33] Depending on the Fermi level, the different charge states will have, in principle, different activation energies for their formation and dissociation. The consequence will thus be the observation of different temperatures for which the corresponding complexes are annealed.

Here, we present detailed results on the lattice location of the transition metal Ni in different types of Si, which were obtained from on-line EC experiments using the short-lived isotope $^{65}$Ni ($t_{1/2}$=2.5 h).

## II. EXPERIMENT

Three Czochralski grown silicon samples were studied: (**i**) lightly doped $n$-type Si ($n$-Si) with a resistivity of 7.3-12 Ω cm, doped with $2\times10^{15}$ cm$^{-3}$ phosphorus; (**ii**) $n^+$-type Si ($n^+$-Si) with a resistivity of (4.5-5.7)$\times10^{-3}$ Ω cm, doped with $2.5\times10^{19}$ cm$^{-3}$ arsenic; (**iii**) $p^+$-type Si ($p^+$-Si) with a resistivity of (1-5)$\times10^{-3}$ Ω cm, doped with $6\times10^{19}$ cm$^{-3}$ boron. All samples had < 111 > surfaces.

$^{65}$Ni was implanted at the on-line isotope separator facility ISOLDE at CERN. ISOLDE provides mass-separated beams of radioactive Ni isotopes, produced by nuclear fission of uranium carbide $UC_2$ targets induced by 1.4 GeV proton beams. A laser ion source was used for chemically selective ionization of the desired el-

ement. Unlike typical EC experiments using long-lived TM isotopes, e.g. $^{59}$Fe, $^{67}$Cu and $^{111}$Ag, where the samples are implanted and measured in different setups, the $^{65}$Ni experiments were carried out using an on-line setup where both implantation and measurement took place.[21] Since the half-life of $^{65}$Ni is relatively short ($t_{1/2}$=2.5 h), carrying out the measurements on-line is indispensable. Therefore, for each experiment, the sample was mounted on a goniometer inside the on-line setup, at the end of one of the ISOLDE general purpose separator beam lines. $^{65}$Ni was implanted before each annealing treatment, into the three samples with an energy of 50 keV, under an angle of 17° from the surface normal in order to avoid channeling implantation. The accumulated fluences were $3.2 \times 10^{13}$ cm$^{-2}$ in $n^+$- and $p^+$-Si and $2.4 \times 10^{13}$ cm$^{-2}$ in $n$-Si. The anneals were performed *in situ* up to 700°C in steps of 100°C, during 10 min, under vacuum better than $10^{-5}$ mbar. The warm-up times were relatively short (under 5 minutes, even for the highest annealing temperatures). The time required to cool the sample down to room temperature (before starting the measurements) was significantly longer, up to 30 minutes for the highest annealing temperatures.

Angular-dependent emission yields of the $\beta^-$ particles emitted during radioactive decay were measured at room temperature, in the vicinity of the $< 110 >$, $< 211 >$, $< 100 >$ and $< 111 >$ directions. These patterns were recorded using a position- and energy-sensitive detection system similar to that described in Ref. 34. As mentioned above, given the relatively short half-life of $^{65}$Ni, this system was installed on-line and upgraded with self-triggering readout chips for the Si pad detectors, enabling measurements during and/or immediately after implantation with count rates of up to several kHz.[21] The electrons that are backscattered into the detector by the chamber walls were accounted for by subtracting an isotropic background, estimated using the Monte Carlo electron scattering simulation code GEANT4.[35]

The depth profile of the implanted $^{65}$Ni and created vacancies were estimated using the SRIM code.[36] The implanted $^{65}$Ni profile is approximately a Gaussian distribution centered at 453 Å with a straggling of 172 Å and a peak concentration of $5{\times}10^{18}$ cm$^{-3}$. At 0 K, each implanted $^{65}$Ni creates $\sim$ 900 vacancies along its path, producing a vacancy depth profile centered approximately half way from the surface to the peak of the implanted $^{65}$Ni concentration. The concentration peak of the vacancy profile is $\sim 5{\times}10^{21}$ cm$^{-3}$.

## III. METHOD OF ANALYSIS

In order to obtain the occupied lattice sites of $^{65}$Ni, the two-dimensional experimental patterns were fitted by using calculated beta emission yields, obtained with the so-called *many beam* formalism for electron channeling in single crystals.[37] In the following it is given a detailed description of the used lattice sites in the analysis, as well as the fitting procedure adopted in this work.

### A. Lattice sites

Theoretical patterns were calculated for $^{65}$Ni emitters in all the relevant high symmetry sites in Si: substitutional (S), hexagonal (H), tetrahedral (T), bond-center (BC), anti-bonding (AB), split (SP) and the so-called DS, DT, Y and C sites. Lower-symmetry sites were also considered, corresponding to displacements between the higher-symmetry ones along the $< 111 >$, $< 100 >$ and $< 110 >$ directions. As examples, which will be useful for the understanding of the experimental patterns below, Fig. 1 (**a**) shows the theoretical emission yield for the S, BC, AB and T sites in the vicinity of the four measured directions. The position of all the mentioned high-symmetry sites in the Si lattice is depicted in Fig. 1 (**b**). We note that the emission channeling technique does not provide information about the immediate neighbourhood of the radioactive $^{65}$Ni probes but rather on their geometrical position with respect to the perfect diamond lattice. The microscopic origin of the observed sites can therefore not be directly inferred from our measurements. In that respect, our use of the term bond-centered (BC) does not imply a position of Ni where it perturbs SiSi covalent bonds, as occurring for the case of hydrogen[38] (Si-$H_{BC}$-Si bond) or oxygen[39] (slightly puckered Si-$O_{BC}$-Si bond), but rather to its geometrical position in the lattice. This position would be the same for instance for Ni atoms disturbing covalent Si-Si bonds in an ideal BC position, or for Ni atoms located in the center of a divacancy.

### B. Fitting procedure

The analysis was started by fitting with one fraction only for each experimental pattern, and only then we added more fractions to the analysis if justified. Therefore, depending on the annealing temperature, two sites gave consistently the lowest value for the $\chi^2$ of fit in the studied three types of silicon: sites in the vicinity of BC sites and sites in the vicinity of T sites. A two fraction fit was then carried out with these two types of sites. The small displacements from S and T sites were adjusted by minimizing the $\chi^2$ of fit as function of these parameters. Since the occupation of ideal S sites by $^{65}$Ni is often mentioned in literature, a three fraction fit was also evaluated by allowing for an extra ideal S fraction to the two fractions mentioned above. The inclusion of the ideal S fraction resulted in a significant decrease of $\chi^2$ , although ideal S sites were not the dominant fraction in any of the fitted patterns. A further adjustment of the near-BC and near-T displacements was then allowed. At this point additional fractions seemed not to reduce the $\chi^2$ of fit considerably. In particular, ideal BC sites were included in a four fraction fit but without a signif-

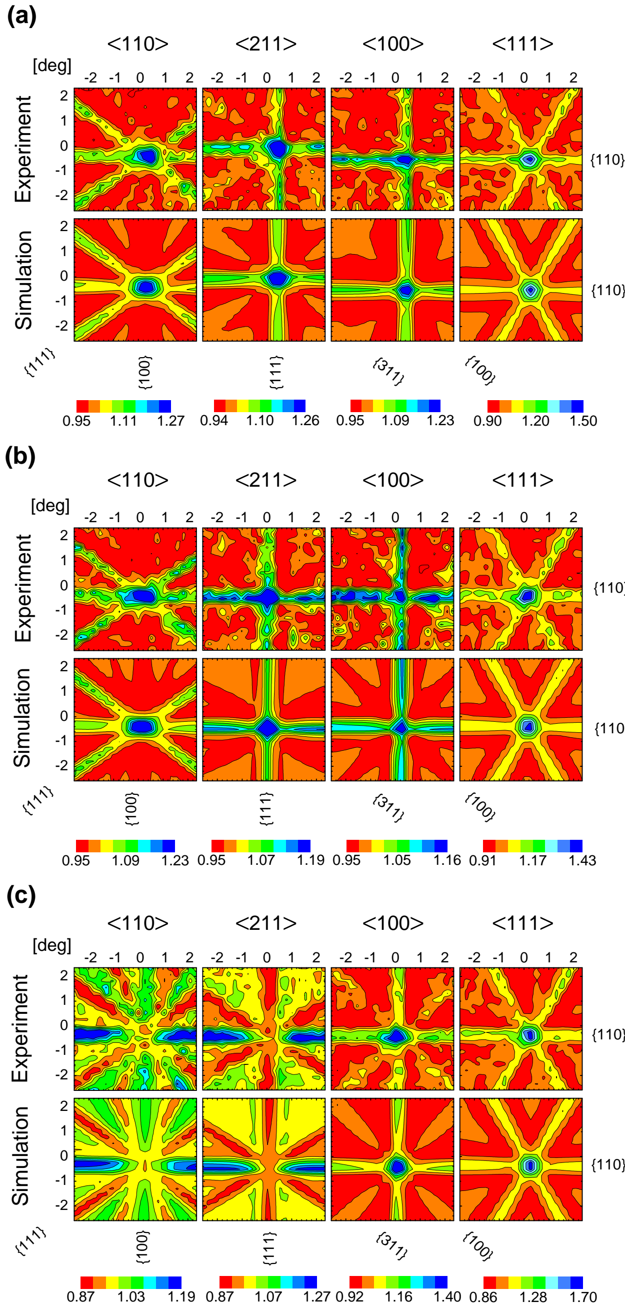


FIG. 2. (Color online) Comparison of the two-dimensional experimental and calculated emission channeling patterns from $^{65}$Ni in $n$-Si. The beta emission yield is represented in the vicinity of $< 110 >$, $< 211 >$, $< 100 >$ and $< 111 >$ following (**a**) implantation at room temperature, (**b**) annealing at 400°C and (**c**) 500°C.

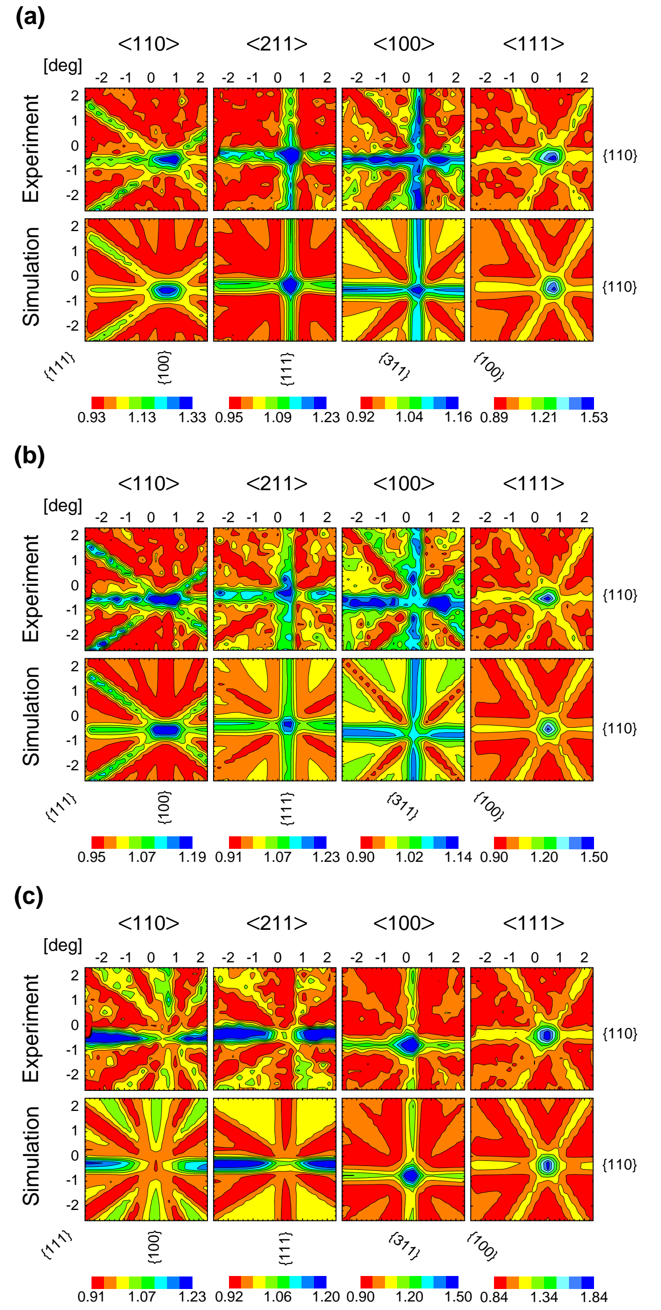


FIG. 3. (Color online) Comparison of the two-dimensional experimental and calculated emission channeling patterns from $^{65}$Ni in $n^{+}$-Si, following (**a**) annealing at 400°C, (**b**) 500°C and (**c**) 600°C.

icant $\chi^2$ reduction. Therefore, the fits were confined to the three lattice sites: ideal S sites; sites displaced from BC towards S sites (near-BC) and sites displaced from T towards AB sites (near-T).

In addition to the high-symmetry sites mentioned so far, which contribute with an anisotropic emission yield, other sites may also be occupied which contribute with a virtually isotropic component, i.e. the *random* fraction (R). R is given by 100% minus the fractions of all regular sites included in the fits. Generally, R is largest in the as-implanted state and decreases with annealing temperature. Note that R will become negative if the sum of all fractions on regular sites grows above 100%. This behavior occurs when the actual $^{65}$Ni profile moves towards the surface compared to the assumed $^{65}$Ni profile,

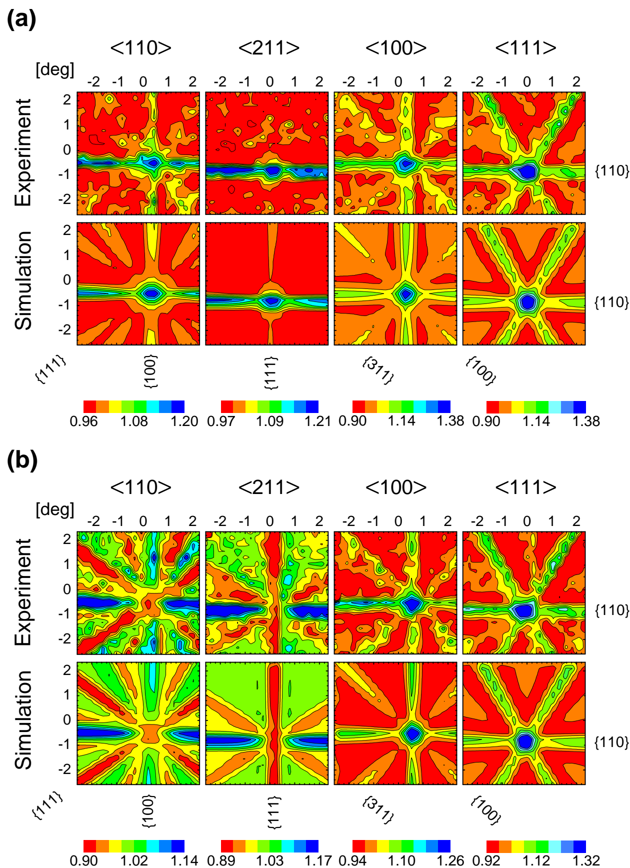


FIG. 4. (Color online) Comparison of the two-dimensional experimental and calculated emission channeling patterns from $^{65}$Ni in $p^+$-Si, following (**a**) annealing at 400°C and (**b**) 500°C.

since the electron channeling is more pronounced when the emission occurs closer to the surface.

## IV. RESULTS

The two-dimensional experimental channeling patterns from $^{65}$Ni in low doped n -Si, $n^+$-Si and $p^+$-Si for various annealing temperatures are shown in Figs. 2, 3 and 4, while the fractions on the three fitted sites as a function of annealing temperature are shown in Fig. 5.

### A. $n$-type Si

In the as-implanted state, the best fits show that 21% of Ni occupies ideal S sites, 22% near-BC sites and 27% near-T sites [Fig. 2 (**a**)]. Note that the patterns show the presence of channeling peaks along all four orientations, characteristic for S sites, and a significant absence of channeling {100} planes, characteristic for the AB and BC sites. Following annealing up to 400°C, only small changes are to be seen in the patterns: {311} and {100} planes in the vicinity of the $< 211 >$ and $< 100 >$ directions become completely blocked, from Fig. 2 (**a**) to (**b**). Furthermore, {111} channeling planes are still present, at least with the same intensity. These two observations suggest an increase of a near-BC fraction, cf. the beta emission yield of BC sites from Fig. 1 (**a**). However, by annealing the sample at 500°C, the vanishing of the channeling peaks of the $< 110 >$ and $< 211 >$ directions [from Fig. 2 (**b**) to (**c**)] clearly shows a site change of $^{65}$Ni to near-T sites. In fact, by fitting the two-dimensional experimental beta emission yield of $^{65}$Ni with the calculated emission yield from the three types of sites, ideal S, near-BC and near-T, one can conclude that after annealing at 400°C the majority of Ni ($\sim$ 43%) sits on near-BC sites, while after annealing at 500°C Ni prefers near-T sites ($\sim$ 54%). After annealing at 600°C, the channeling effects are no longer observed, suggesting long-range diffusion of $^{65}$Ni. The displacements, given by the best fits, from the ideal BC and T sites are plotted in Fig. 6 as a function of annealing temperature. Both near-BC and near-T displacements seem to be stable against annealing, around 0.25 Å for near-BC sites and 1.18 Å for near-T sites. These strongly displaced near-T sites are, in fact, very close to the ideal AB site. Only for the 500°C annealing step, the near-T sites are clearly off the AB site. In fact, at this annealing temperature we can observe a pronounced peak along the $< 100 >$ direction [Fig. 2 (**c**)], characteristic of the ideal T rather than AB sites [Fig. 1 (**a**)].

### B. $n^+$-type Si

Figure 3 shows the two-dimensional experimental patterns from $^{65}$Ni in $n^+$-Si following annealing at 400°C, 500°C and 600°C. The fraction dependence on the annealing temperature is plotted in Fig. 5 (**a**). A similar behavior of the patterns compared to those from low-doped $n$-Si is exhibited, in particular with similar fractions for the three lattice sites occupied by $^{65}$Ni after room temperature implantation. Nevertheless, the site change of $^{65}$Ni from near-BC to near-T sites occurs here at 600°C. Also, after annealing the silicon sample at 500°C [Fig. 3 (**b**)] one can observe more intense blocking effects of the {311} and {100} planes and a significant decrease of the channeling peak from the $< 100 >$ direction, suggesting a larger near-BC fraction compared to that of $n$-Si. After the 600°C anneal [Fig. 3 (**c**)] the channeling peaks from the $< 110 >$ and $< 211 >$ directions disappear while that from $< 100 >$ becomes more intense, showing evidence of an increase of the near-T fraction: the best fit results show that after the 500°C anneal $^{65}$Ni prefers near-BC sites ($\sim$ 64%), while after the 600°C anneal the majority of $^{65}$Ni ($\sim$ 76%) sits on near-T sites. From Fig. 6 one can also observe a similar dependence of the displacements from BC and T sites on the annealing temperature compared to those from $n$-Si. While near-BC sites are very close to the ideal BC site

in the whole range of the annealing temperature, near-T sites are located close to AB sites up to 500°C, changing to sites closer to the ideal T site at 600°C. Finally, channeling effects disappear at 700°C, which suggests $^{65}$Ni long-range diffusion.

### C. $p^+$-type Si

The experimental EC patterns from $^{65}$Ni in $p^+$-Si are shown in Fig. 4 after annealing at 400°C and 500°C. Once more, a similar behavior with the annealing temperature is observed as for the other doping types. Nevertheless, after the 400°C anneal, the experimental patterns exhibit a less pronounced channeling effect of the {111} plane in the vicinity of the $< 110 >$ and $< 211 >$ directions. This fact indicates a higher near-T fraction already at 400°C in comparison to the other two samples, with $\sim 27\%$ of the $^{65}$Ni atoms on near-T sites. Similarly to the $n$-Si experiment, the near-T fraction reaches its maximum value after annealing at 500°C [Fig. 4 (**b**)], where the fraction of $^{65}$Ni on near-T sites increases to $\sim 51\%$. However, the near-T fraction does not drop to a value close to zero after the 600°C anneal. Instead, it decreases to $\sim 35\%$. The annealing temperature required for long-range diffusion of Ni was therefore probably not reached in this type of sample. The displacement from the BC sites is again stable with the annealing temperature, $^{65}$Ni sitting close to BC sites in the whole temperature range. A more complex dependence is, however, observed for the near-T sites. In fact, from Fig. 6, one can see that near-T sites are close to AB sites, but an anneal of 200°C pushes the near-T sites towards the ideal T position, where they remain up to the annealing temperature of 600°C.

## V. DISCUSSION

Using similar arguments as outlined for the case of $^{59}$Fe in Si in Ref. 19, it appears that only vacancies, self interstitials and the formation of $^{65}$Ni clusters might be responsible for the confinement of $^{65}$Ni at the channeling region. As was suggested by a recent theoretical study[6] vacancies are very stable traps for Ni, while interactions with Si interstitials, C and O impurities or other Ni atoms seem to play only a minor role. In the following subsections we discuss the origin of the lattice sites of $^{65}$Ni as well as the evidence of $^{65}$Ni trapping into defects at the $R_p/2$ region and the influence of the doping on their thermal stability. Finally, a comparison to other EC studies involving transition metals is given.

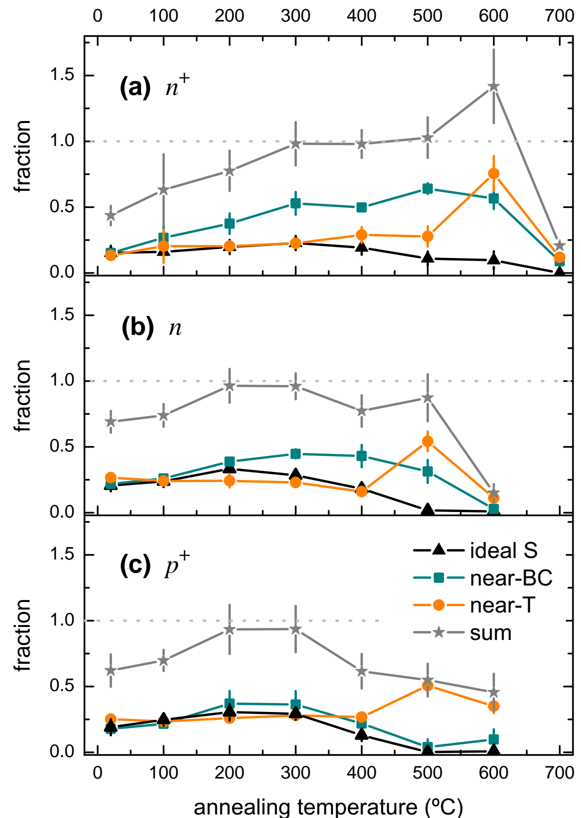


FIG. 5. Fractions of $^{65}$Ni on the ideal S, near-BC and near-T sites as a function of annealing temperature, in (**a**) $n^+$-, (**b**) $n$- and (**c**) $p^+$-Si.

### A. Lattice location

#### 1. Ideal S sites

Although some energy levels from DLTS studies have been assigned to substitutional Ni,[5,13,40] an unambiguous proof for its existence could never be established. Here, we can show that substitutional Ni is indeed stable. One should note, however, that this substitutional fraction is likely to result from the high concentration of single vacancies that is introduced during Ni implantation.

#### 2. Near-BC sites

The origin of the near-BC sites seems to be related to the $^{65}$Ni interaction with multivacancies. For clusters constituted by only two vacancies, ideal BC sites might be preferred over other positions.[41,42] On the other hand, for vacancy clusters constituted by more than two vacancies, e.g. 3-6 vacancy clusters, the structural rearrangement after their formation can, for instance, result in a fourfold configuration based on hexavacancy rings where

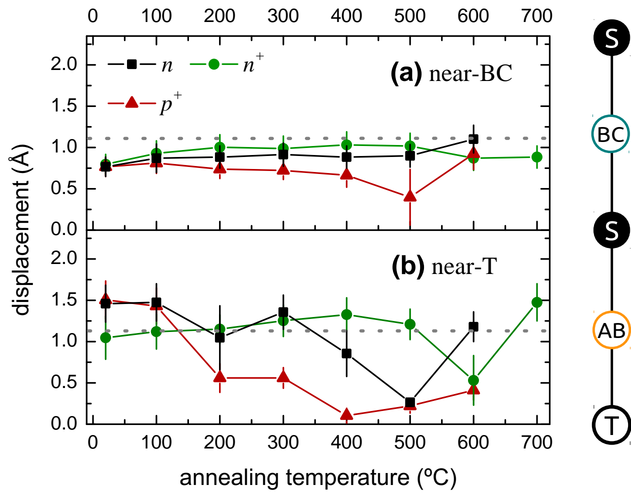


FIG. 6. Displacement of (**a**) near-BC and (**b**) near-T sites along the <111> direction as a function of annealing temperature, in $n$-, $n^+$- and $p^+$-Si.

extra Si atoms are incorporated near BC positions to satisfy dangling bonds.[43] Similar geometries were also proposed when hexavacancies are filled up by Cu atoms.[44] It should thus be feasible that other transition metals such as Ni might be incorporated, perhaps along with self interstitials from the $R_p$ region, into multivacancies based on hexavacancy rings, and be stable on near-BC sites. The final result would hence be a near-BC fraction constituted by a mixture of $^{65}$Ni inside divacancies, occupying ideal BC sites, and $^{65}$Ni inside more complex multivacancies, occupying off-BC sites. Note that because the displacements from the BC sites are small, it is hard to distinguish these two complexes during the fitting procedure. Moreover, as pointed out, the effect on $\chi^2$ of adding an additional fraction to the other three would be very small, and therefore inconclusive.

#### 3. Near-T sites

The trapping mechanism of $^{65}$Ni atoms on near-T sites is more complex than that on ideal S or near-BC sites. This fact is evident from Fig. 6 (**b**) showing the dependence of the displacement from ideal T towards AB sites with the annealing temperature, which suggests the existence of different complex structures with $^{65}$Ni sitting on near-T sites. Though in $n^+$- and $n$-Si the position varies considerably with annealing temperature, we can classify the related complexes into two classes of $^{65}$Ni displacements from the ideal T site:
(**i**) $^{65}$Ni on ideal AB sites,
(**ii**) $^{65}$Ni close to ideal T sites.
In $p^+$-Si, $^{65}$Ni behaves in a different way and therefore cannot be described in terms of these two classes. In fact, although decreasing from the ideal AB site to the ideal T site with the annealing temperature, as in $n^+$ and $n$-Si, the $^{65}$Ni displacement changes more gradually rather than abruptly. It seems, however, feasible that the intermediate displacements, at the annealing temperatures of 200°C and 300°C, could result from a mixture of $^{65}$Ni atoms trapped by the two discussed classes of complexes. The origin of these sites might be again related to $^{65}$Ni interactions with vacancy-type defects. As an example, it is known that although ideal S and BC sites are the preferred positions when Fe is trapped into single and double vacancies in silicon, respectively, near-T sites also present some stability.[18,41] Ni may thus behave in a similar way. While the participation of self-interstitials as well as the formation of $^{65}$Ni clusters cannot be ruled out, both have recently been suggested to be not very effective from an energetic point of view[6]. Because of the reasons pointed out above we conclude that a complete picture of the structure of the complexes in which Ni occupies near-T sites is difficult to obtain. We can nevertheless present some of their characteristics as well as their thermal stability, which will be discussed in more detail in the subsections **B** and **C**.

### B. $^{65}$Ni profile

Eventual changes in the $^{65}$Ni depth profile upon thermal annealing can be inferred from changes in intensity of the channeling effects, i.e. from changes in the sum of the three fitted fractions. If the $^{65}$Ni profile starts to change, e.g. due to dissociation of the complexes in the $R_p$ region, the intensity of the channeling effects will in principle also change. If the profile moves to the bulk, channeling effects are reduced and thus the sum fraction decreases. On the other hand, if the $^{65}$Ni profile moves towards the surface, the channeling effects are enhanced and the sum fraction can increase to values above 100%. This is what probably happened in $n^+$-Si [Fig. 5 **(a)**]. A fraction of $^{65}$Ni might have started to diffuse from the $R_p$ region, after dissociating from the observed lattice sites, towards the surface, and be trapped into other defects. This explanation is consistent with the so called "$R_p/2$ effect" in which Ni is gettered into defects at the $R_p/2$ region of the wafer, rich in vacancy-type defects resulting from implantation.[31,32] This behavior seems to be also present in $n$-Si and $p^+$-Si after annealing at 500°C, but to a lesser extent since the fraction sum never attains values above 100%.

An important information that we can extract from our emission channeling experiments is the lattice sites where $^{65}$Ni sits at the $R_p/2$ region. In that respect, we can observe a prevailing near-T fraction when the sum increases in $n$- and $n^+$-Si or decreases at a lower rate in $p^+$-Si, at the annealing temperatures of 500-600°C. Moreover, during the relocation of $^{65}$Ni, the displacement of the near-T sites seems to change from the ideal AB site to sites closer to the ideal T site in $n$- and $n^+$-Si. The same change of displacement is again observed in $p^+$-Si but more gradually. Within this scenario such a change

might be explained either by a different channeling effect of the relocated $^{65}$Ni profile, that is not considered in our simulated patterns, or by the presence of a different trap structure at $R_p/2$ compared to those of the $R_p$ region.

Summarizing, although we do not have access to the complete structure of the traps, it appears that a fraction of $^{65}$Ni atoms, that is dissociated from the sites at the $R_p$ region, is retrapped on near-T sites at $R_p/2$. This retrapping occurs in the narrow window of 100°C after annealing at 500-600°C. The observed change of displacement of the near-T sites might be a consequence of this transition.

### C. Influence of the doping on the thermal stability

From Fig. 5 one can observe different lattice sites prevailing at different annealing temperatures, as a result of their distinct thermal stabilities. By using an Arrhenius model described in , e.g., Refs. 17, 19, and 23, one can estimate the activation energies $E_D$ for the $^{65}$Ni dissociation from each of the three observed lattice sites with the formula:

$$E_D = k_B T \log\left[\frac{\nu_0 \Delta t}{N}\frac{1}{\log\left(\frac{f_{n-1}}{f_n}\right)}\right], \quad (1)$$

where $\nu_0$ is the attempt frequency, $\Delta t$ the annealing time, $T$ the annealing temperature, $f_n$ the fraction after annealing at $T$, $f_{n-1}$ the fraction before the anneal at $T$, and $N$ the required number of steps for $^{65}$Ni to go to another type of trap or to escape from the channeling region. Table I shows the values obtained for the three observed lattice sites. We could not find, however, a reliable value for $E_D$ of $^{65}$Ni on ideal S sites in $n^+$-Si, due to the difficulty in identifying at which temperature the fraction starts to decrease [see Fig. 5 (**a**)]. Note also that, although it is not possible to conclude accurately on the thermal stability of near-T sites at the $R_p$ region, we can estimate activation energies for $^{65}$Ni dissociation from the $R_p/2$ region.

It is clear from Table I that the activation energy for dissociation of $^{65}$Ni from near-BC sites changes with the doping, increasing from $p^+$-Si to $n$-Si and further to $n^+$-Si. The values in Table I show also that the thermal stability of near-T sites at the $R_p/2$ region does not change much with the doping. Furthermore, by comparing the near-T sites to the behavior of Ni at $R_p/2$ from Ref. 8, one can conclude that a lower concentration of vacancies leads to a smaller gettering efficiency. In fact, when using fluences of implanted Si of $\sim 1\times10^{15}$ cm$^{-2}$, Ni shows thermal stability at $R_p/2$ up to the temperature of 900°C, while in our case $^{65}$Ni, implanted with fluences of $\sim 1\times10^{13}$ cm$^{-2}$, dissociates already at 600°C. Finally, the estimated activation energies for dissociation of $^{65}$Ni from ideal S sites seem not to change from $p^+$- to $n$-Si, showing a value ranging from 1.6 eV to 2.0 eV. These values are smaller than the estimate $\sim$ 3 eV from first principle calculations.[5]

TABLE I. Estimated activation energies for dissociation of $^{65}$Ni from near-BC, near-T and ideal S sites, in the three types of silicon.

| Defect | $p^+$-type Si | $n$-type Si | $n^+$-type Si |
|---|---|---|---|
| ideal S | 1.8-2.0 eV | 1.6-1.8 eV | - |
| near-T | 2.4-2.6 eV | 2.3-2.5 eV | 2.5-2.8 eV |
| near-BC | 1.8-2.0 eV | 2.1-2.3 eV | 2.5-2.7 eV |

### D. Comparison to other transition metals

In this subsection we discuss the similarities and differences between the present emission channeling work on $^{65}$Ni with those on $^{59}$Fe,[17–19] $^{67}$Cu[14–16] and $^{111}$Ag.[20] While both $^{67}$Cu and $^{59}$Fe were investigated in lightly and heavily doped $n$- and $p$-type silicon, $^{111}$Ag was only studied in two light doping types. $^{59}$Fe was the only transition metal that was identified on the same three types of lattice sites observed in this work. $^{67}$Cu was identified on near-S and ideal S sites, and $^{111}$Ag on near-S and near-T sites.

Near-S and near-BC sites can be considered as being part of the same type of sites since they only differ in their distances from the S or BC sites, along the <111> direction [see Fig. 1 (**b**)]: near-BC sites are closer to BC while near-S sites are closer to S. It is evident that the three transition metals Ni, Fe and Cu start their dissociation in $n^+$-Si from near-BC or near-S sites in the same range of temperatures (500-600°C). Furthermore, they show a change of thermal stability with the doping when sitting on near-S or near-BC sites, increasing from $p^+$- to $n$- and further to $n^+$-Si. We can therefore conclude that the nature of the transition metal does not play a major role on the trapping mechanism into near-S and near-BC sites. This might be relevant for the understanding of the microscopic mechanism of P-diffusion gettering, which is used for a *wide* number of transition metals and in which vacancy-related defects have been suggested to play a role.[11,45]

The evidence of $^{65}$Ni trapping on near-T sites at $R_p/2$ has similarities with the $^{59}$Fe behavior on near-T sites in lightly doped Si. In fact, the increase of the near-T fraction is also accompanied with a sum of all the fractions to values above 100%. Although the dependence of the displacement from the ideal T site was not studied at that time, since simulations were only available for a small number of displacements, it was clear that a reshaping of the $^{59}$Fe profile was taking place at high temperatures. A particular feature of the near-T sites of $^{59}$Fe in $p^+$-Si was its prevalence over the other two fractions in the whole annealing temperature range. It was suggested that the mobile $^{59}$Fe, predominantly positively charged in $p^+$-Si, might be trapped by immobile $B^-$ acceptors, on near-T

sites. This observation contrasts with that of Ni. Indeed, Ni prevails in the neutral charge state when diffusing interstitially, which makes such interactions between interstitial $Ni^0$ and $B^-$ unlikely. This might explain why Ni does not prevail in $p^+$-Si on near-T sites in the whole annealing temperature range, as observed for $^{59}$Fe.

Finally, we should note that although also detected in $^{59}$Fe and $^{67}$Cu studies, ideal S sites seem to have different thermal stabilities. While an activation energy of 3.5 eV for dissociation of $^{59}$Fe from ideal S sites was obtained in Ref. 17, compared to the 3.0 eV from the theoretical grounds of Ref. 5, $^{67}$Cu seemed to need 2.9 eV to dissociate,[17] compared to the first principle calculated value of 2.8 eV from Ref. 42. The experimental value for $^{65}$Ni dissociation from ideal S sites (Table I) is thus the lowest among the three discussed transition metals.

## VI. CONCLUSION

We have experimentally identified $^{65}$Ni on three different lattice sites: ideal S, near-BC and near-T sites. Arguments have been presented to assign the trapping of $^{65}$Ni into implantation defects to the majority of the three observed lattice sites. This study shows an appreciable thermal stability of Ni on ideal S sites in silicon, for which the activation energy for Ni dissociation 1.6-2.0 eV was obtained. A significant fraction of $^{65}$Ni seems to be also trapped into multivacancies on near-BC sites, such as into divacancies and fourfold vacancy clusters based on hexavacancy rings. Because the thermal stability of near-BC sites is similar to those of $^{59}$Fe, $^{67}$Cu and $^{111}$Ag, we show that the nature of the transition metal does not play a major role on the related trapping mechanism. In particular, the thermal stability of near-BC sites seems to change with the doping, increasing from $p^+$- to $n$- and further to $n^+$-Si. The high thermal stability of near-BC sites in $n^+$-Si shall hence have an important role not only on the P-diffusion gettering of Fe but also on that of Ni. Although the three lattice sites were found to coexist at $R_p$, we identified $^{65}$Ni at the vacancy rich region $R_p/2$ on near-T sites. Finally, unlike Fe that is confined at the channeling region even at 900°C, long-range diffusion of $^{65}$Ni was observed already at 600-700°C. Vacancy-related defects seem therefore to be less thermally stable in gettering Ni than Fe.

## ACKNOWLEDGMENTS

This work was supported by "Fundação para a Ciência e Tecnologia" (FCT), Portugal (CERN-FP-123585-2011) and by the European Commission $7^{\text{th}}$ Framework through ENSAR (European Nuclear Science and Applications Research, Contract No. 262010). Project Norte-070124-FEDER-000070 is acknowledged. D.J. Silva is thankful for FCT Grant (SFRH/BD/69/435/2010). The authors thank the ISOLDE collaboration for providing highly pure $^{65}$Ni beams.

[1] E. R. Weber, Appl. Phys. A **30**, 1 (1983)
[2] D. MacDonald, Appl. Phys. A **81**, 1619 (2005)
[3] A. A. Istratov, T. Buonassisi, R. J. McDonald, A. Smith, R. Schindler, J. A. Rand, J. P. Kalejs, and E. R. Weber, J. Appl. Phys. **94**, 6552 (2003)
[4] S. Pizzini, Sol. Energy Mater. Sol. Cells **94**, 1528 (2010)
[5] D. J. Backlund and S. K. Estreicher, Phys. Rev. B **81**, 235213 (2010)
[6] J. Lindroos, D. P. Fenning, D. J. Backlund, E. Verlage, A. Gorgulla, S. K. Estreicher, H. Savin, and T. Buonassisi, J. Appl. Phys. **113**, 204906 (2013)
[7] D. J. Backlund and S. K. Estreicher, Phys. Rev. B **82**, 155208 (2010)
[8] R. A. Brown, O. Kononchuk, G. A. Rozgonyi, S. Koveshnikov, A. P. Knights, P. Simpson, and F. Gonzlez, J. Appl. Phys. **84**, 2459 (1998)
[9] S. M. Myers, D. M. Follstaedt, and D. M. Bishop, Materials Research Society Symposium Proceedings **316**, 33 (1994)
[10] A. Ourmazd and W. Schröter, Applied Physics Letters **45**, 781 (1984)
[11] S. M. Myers, M. Seibt, and W. Schröter, J. Appl. Phys. **88**, 3795 (2000)
[12] A. A. Istratov, P. Zhang, R. J. McDonald, A. R. Smith, M. S. J. Moreland, J. Shen, R. Wahlich, and E. R. Weber, J. Appl. Phys. **97**, 023505 (2005)
[13] A. A. Istratov and E. R. Weber, Appl. Phys. A **66**, 123 (1998)
[14] U. Wahl, J. G. Correia, A. Vantomme, and G. Langouche, Physica B **273-274**, 367 (1999)
[15] U. Wahl, A. Vantomme, G. Langouche, J. P. Araújo, L. Peralta, and J. G. Correia, Appl. Phys. Lett. **77**, 2142 (2000)
[16] U. Wahl, A. Vantomme, G. Langouche, and J. G. Correia, Phys. Rev. Lett. **84**, 1495 (2000)
[17] U. Wahl, J. G. Correia, E. Rita, J. P. Araújo, and J. C. Soares, Nucl. Instrum. Methods. Phys. Res. Sect. B **253**, 167 (2006)
[18] U. Wahl, J. G. Correia, E. Rita, J. P. Araújo, and J. C. Soares, Phys. Rev. B **72**, 1 (2005)
[19] D. J. Silva, U. Wahl, J. G. Correia, and J. P. Araújo, J. Appl. Phys. **114**, 103503 (2013)
[20] U. Wahl, J. G. Correia, and A. Vantomme, Nucl. Instrum. Methods. Phys. Res. B **190**, 543 (2002)
[21] M. R. da Silva, U. Wahl, J. G. Correia, L. M. Amorim, and L. M. C. Pereira, Rev. Sci. Instrum. **84**, 073506 (2013)
[22] S. Decoster, S. Cottenier, U. Wahl, J. G. Correia, L. M. C. Pereira, C. Lacasta, M. R. D. Silva, and A. Vantomme, Appl. Phys. Lett. **97**, 151914 (2010)
[23] L. M. Pereira, U. Wahl, S. Decoster, J. G. Correia, M. R. da Silva, A. Vantomme, and J. P. Araújo, Appl. Phys. Lett. **98**, 201905 (2011)
[24] L. M. C. Pereira, U. Wahl, S. Decoster, J. G. Correia, L. M. Amorim, M. R. D. Silva, J. P. Araújo, and A. Vantomme, Phys. Rev. B **86**, 125206 (2012)
[25] L. M. C. Pereira, U. Wahl, J. G. Correia, S. Decoster, L. M. Amorim, M. R. D. Silva, J. P. Araújo, and A. Vantomme, Phys. Rev. B **86**, 195202 (2012)
[26] L. M. C. Pereira, U. Wahl, S. Decoster, J. G. Correia, L. M. Amorim, M. R. D. Silva, J. P. Araújo, and A. Vantomme, Phys. Rev. B **84**, 125204 (2011)
[27] L. M. C. Pereira, U. Wahl, J. G. Correia, L. M. Amorim, D. J. Silva, E. Bosne, S. Decoster, M. R. da Silva, K. Temst, and A. Vantomme, Appl. Phys. Lett. **103**, 091905 (2013)
[28] B. Mohadjeri, J. S. Williams, and J. Wong-Leung, Appl. Phys. Lett. **66**, 1889 (1995)
[29] S. Koveshnikov and O. Kononchuk, Appl. Phys. Lett. **73**, 2340 (1998)
[30] A. Peeva, R. Kögler, and W. Skorupa, Nucl. Instrum. Methods. Phys. Res. B **206**, 71 (2003)

[31] J. S. Williams, M. J. Conway, B. C. Williams, and J. Wong-Leung, Appl. Phys. Lett. **78**, 2867 (2001)
[32] A. Peeva, R. Kögler, W. Skorupa, J. S. Christensen, and A. Y. Kuznetsov, J. Appl. Phys. **95**, 4738 (2004)
[33] H. Kitagawa, S. Tanaka, H. Nakashima, and M. Yoshida, J. Electron. Mater. **20**, 441 (1991)
[34] U. Wahl, J. G. Correia, A. Czermak, S. G. Jahn, P. Jalocha, J. G. Marques, A. Rudge, F. Schopper, J. C. Soares, A. Vantomme, and P. Weilhammer, Nucl. Instrum. Methods Phys. Res. A **524**, 245 (2004)
[35] S. Agostinelli and *et. al.*, Nucl. Instrum. Methods Phys. Res. A **506**, 250 (2003)
[36] J. F. Ziegler, Nucl. Instrum. Methods Phys. Res. B **219-220**, 1027 (2004)
[37] U. Wahl, J. G. Correia, S. Cardoso, J. G. Marques, A. Vantomme, and G. Langouche, Nucl. Instrum. Methods. Phys. Res. Sect. B **136-138**, 744 (1998)
[38] T. L. Estle, S. Estreicher, and D. S. Marynick, Phys. Rev. Lett. **58**, 1547 (1987)
[39] J. W. Corbett, R. S. McDonald, and G. D. Watkins, J. Phys. Chem. Solids **25**, 873 (1964)
[40] M. Shiraishi, J. Sachse, H. Lemke, and J. Weber, Mater. Sci. Eng. B-Adv. Funct. Solid-State Mater. **58**, 130 (1999)
[41] S. K. Estreicher, M. Sanati, and N. G. Szwacki, Phys. Rev. B **77**, 125214 (2008)
[42] S. K. Estreicher, Mater. Sci. Semicond. Process. **7**, 101 (2004)
[43] D. V. Makhov and L. J. Lewis, Phys. Rev. Lett. **92**, 255504 (2004)
[44] S. K. Estreicher, Phys. Rev. B **60**, 5375 (1999)
[45] M. Syre, S. Karazhanov, B. R. Olaisen, A. Holt, and B. G. Svensson, J. Appl. Phys. **110**, 024912 (2011)